IEEE Access
Multidisciplinary | Rapid Review | Open Access Journal

Received July 4, 2020, accepted July 16, 2020, date of publication July 20, 2020, date of current version July 31, 2020.

Digital Object Identifier 10.1109/ACCESS.2020.3010564

A Spatial-Motion Assist-as-Needed Controller for the Passive, Active, and Resistive Robot-Aided Rehabilitation of the Wrist

CHING-HUI LIN, YIN-YU SU, YU-HSUAN LAI, AND CHAO-CHIEH LAN, (Senior Member, IEEE)
Department of Mechanical Engineering, National Cheng Kung University, Tainan 70101, Taiwan

Corresponding author: Chao-Chieh Lan (cclan@mail.ncku.edu.tw)

This work was supported by the Ministry of Science and Technology, Taiwan, under Project MOST 108-2218-E-006-002.

ABSTRACT Demand for robot-assisted therapy has increased at every stage of the neurorehabilitation recovery. This paper presents a controller that is suitable for the assist-as-needed (AAN) training of the wrist when performing the spatial motion. A compact wrist exoskeleton robot is presented to realize the AAN controller. This wrist robot includes series elastic actuators with high torque-to-weight ratios to provide accurate force control required for the AAN controller. In addition to assist-as-needed rehabilitation, the parameters of the AAN controller can be adjusted to deliver passive, active, or resistive rehabilitation. Experimental results demonstrate that the proposed AAN controller can provide the total solution to cover each stage of wrist spatial-motion rehabilitation.

INDEX TERMS Force control, rehabilitation robot, assist-as-needed rehabilitation, series elastic actuator, spatial-motion.

I. INTRODUCTION

Rehabilitation robots can be used to assist the human limb motion. They have been demonstrated to provide repeated and progressive rehabilitation training required for the effective recovery of patients with limb disabilities. To meet the requirement of assistance at different rehabilitation stages, active or passive rehabilitation robots of multiple degrees-of-freedom (DoFs) have been developed to assist the motion of human upper limbs [1]–[13] or lower limbs [14]–[18]. Compared with end-effector type robots [2], [11]–[13], [18], exoskeleton type robots [1], [3], [10], [14]–[17] can provide direct assistance and recovery evaluation at each human joint.

According to the definition of Brunstrom [19], patients in the early stages of neuromuscular injury recovery can hardly move their limbs. Their limbs are passive (flaccid) and require therapists or robots to repeatedly guide the limbs to follow strict patterns. A stiff position controller is required for this type of passive training method. As the patient's limb regains partial voluntary motion, the passive training method becomes less effective because it ignores a patient's participation. There is a need to develop a controller that can maximize the benefit of patient engagement. If the patient needs assistance or correction depending on the direction of motion, the controller can provide adaptive assistance or correction at only the required level, but not more. Assist-as-needed (AAN) controllers, also known as assistive or corrective controllers, have been developed to satisfy such need. AAN controllers have been used in upper limb robots [4], [8]–[12] or lower limb robots [15], [16] to stimulate patients to actively participate.

There are two impedance-based AAN controllers. The band-type controller establishes the inner and outer boundaries as the virtual walls that enforce the human limb motion to lie within the band zone where the robot is in the zero impedance mode. The window-type controller has a desired trajectory and a circular window moving along the trajectory. If the human limb trajectory lies outside the moving window, then the predefined force field will be applied to the human limb to move the limb trajectory back into the window. For the band-type controller, the human limb may idle because it only needs to stay in the band zone. In contrast, the window-type controller (e.g., [11], [12], [15], [16]) can reduce potential idling since the human limb must follow a specific time-dependent trajectory.

To allow human and robot movement to coexist safely, accurate interface force sensing and control are necessary. Various sensors [10], [20]–[22] have been used to detect

The associate editor coordinating the review of this manuscript and approving it for publication was Kang Li.

the intention of the human limb. Due to the limited space around the limb, adding an external force sensor would be inconvenient. To reduce the complexity of rehabilitation, force estimation and control methods without using external force sensors have been adopted [6]–[9]. To more accurately control the interaction force, series elastic actuators (SEAs) have been used [1]–[3], [13], [14], [20].

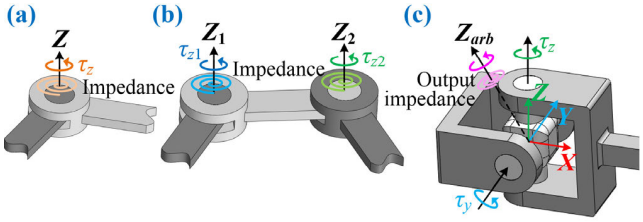

FIGURE 1. AAN motion types. (a) 1-DoF planar motion. (b) 2-DoF planar motion. (c) 2-DoF spatial motion.

This paper presents an AAN controller for a wrist exoskeleton robot [3] to allow the rehabilitation participation of patients with wrist disabilities. Rehabilitation of the human wrist requires 2 or 3-DoF spatial motion around the wrist joint. However, previous AAN controllers mainly focused on the assistance of human joints that make 1-DoF planar motion like the kinematic model in Fig. 1(a). Examples include wrist flexion/extension [9], elbow [10], and knee [16] joints. Other AAN controllers focused on the assistance of human joints that make 2-DoF planar motion like that in Fig. 1(b). Examples include the upper limb [11], [12] and the lower limb [15]. AAN controllers that can be used to directly assist the 2-DoF or 3-DoF spatial motion of a human joint remain under-explored. Such spatial motion includes shoulder, wrist [4], or ankle that can be described using the kinematic model shown in Fig. 1(c). Specifically, the proposed spatial-motion AAN controller offers the following contributions:

- In Fig. 1(a) and 1(b), each assistance torque (τ_z, τ_{z1}, or τ_{z2}) from the planar-motion AAN controller is independent and always aligned with the output impedance direction (represented using a virtual torsional spring) regardless of the number of DoFs. In Fig. 1(c), the two assistance torques of the spatial-motion AAN controller are denoted as τ_y and τ_z. Depending on the time-dependent training trajectory, the magnitudes of the two torques need to be constantly varied in order to synthesize an output impedance along an arbitrary axis $\boldsymbol{Z_{arb}}$. Controlling the direction and magnitude of the output impedance allows accurate spatial-motion assistance. However, generating the output impedance along $\boldsymbol{Z_{arb}}$ is not as straightforward as those in planar-motion AAN controllers. The proposed spatial-motion AAN controller can handle the rehabilitation assistance of more complex human joints.
- Previous AAN controllers focused on assist-as-needed rehabilitation and had rarely shown the ability to achieve passive, active, or resistive rehabilitation. Although a controller can be developed for each rehabilitation stage and switching between controllers is possible [2], using a single controller for the entire rehabilitation process can certainly provide the simplicity of software design and ease of user operation. The developed AAN controller could be used for all the rehabilitation stages.

In what follows, we first describe the mechanical design and kinematics of the wrist robot in Sec. II. The dynamic analysis and force controller design are presented in Sec. III. Sec. IV presents the development of the assistance torque as the basis for the spatial-motion AAN controller. Finally, four experiments are presented in Sec. V to show the effectiveness of the AAN controller in every stage of human wrist rehabilitation.

II. DESCRIPTION OF THE WRIST ROBOT

Fig. 2 shows a prototype of the wrist robot developed in our previous work [3]. It is a parallel robot that has three identical motors rigidly connected to the same frame. The three motors provide the flexion/extension (FE), radial/ulnar deviation (RU), and pronation/supination (PS) of the human wrist. The FE and RU motors provide the output FE and RU rotations of the wrist. As shown in Fig. 2(a), these rotations are defined as θ_p and θ_y, respectively. The output FE and RU torques are denoted as τ_p and τ_y. The wrist PS rotation is provided by the PS motor and the PS geared bearing. The three wrist motors are together rotated θ_s about the forearm to generate the PS rotation.

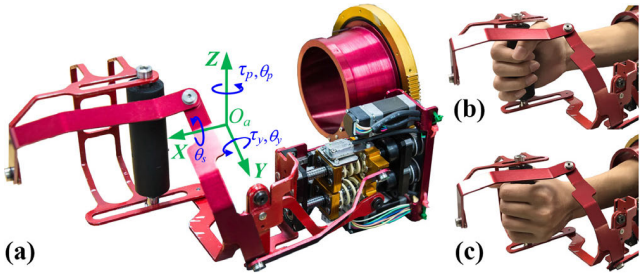

FIGURE 2. (a) Side view of the wrist robot. (b) Right-hand view. (c) Left-hand view.

The total weight of the robot excluding the power supply is 1.5 kg. The motors are placed away from the wrist center to minimize the inertia load and increase device compactness. When compared with previous end-effector type wrist robots [11] and [12] or exoskeleton type wrist robots [4]–[7], [9], the weight and size of our wrist robot are relatively smaller. Yet, the performance of our wrist robot is not compromised. The ranges of rotation are $\theta_p = -70°\sim70°$, $\theta_y = -50°\sim50°$, and $\theta_s = -75°\sim75°$. The average FE, RU, and PS torques are 3.33, 7.54, and 7.13 Nm, respectively.

Series elastic actuators (SEAs) are used for the FE, RU, and PS rotations. By controlling the deformation of a serially connected spring, an SEA can provide accurate force control, back-drivability, and adjustable impedance without

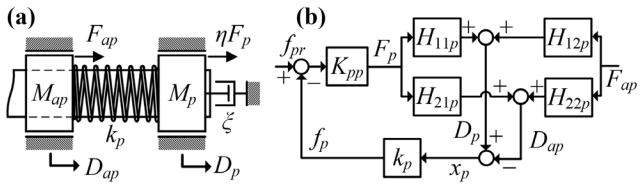

FIGURE 3. (a) Dynamic model of the FE SEA. (b) FE force controller diagram.

using additional force sensors [23]. The reduction of additional force sensors also makes the wrist robot more compact and lightweight. For clarity of presenting the spatial-motion AAN controller, we focus here on the assistance of using the FE and RU SEAs of the wrist robot.

III. DYNAMICS AND CONTROL

A. DYNAMIC MODEL AND FORCE CONTROLLER

Fig. 3(a) shows the FE SEA dynamic model. The FE motor produces the equivalent ball screw force ηF_p where η is the efficiency coefficient that takes into account the Coulomb friction of the screw. The force F_{ap} is provided by the human wrist. These two forces are the inputs. The viscous damping coefficient due to the ball screw and linear guides is denoted as ξ. Symbol M_p denotes the reflected rotor mass of the motor and M_{ap} is the reflected output mass from the hand and wrist robot as seen by the FE motor. The mass M_p is connected to the ball screw, whereas M_{ap} is connected to M_p through the series spring. The dynamics of the FE rotation can be derived as

$$\eta F_p - k_p x_p = M_p \ddot{D}_p + \xi \dot{D}_p; \quad F_{ap} + k_p x_p = M_{ap} \ddot{D}_{ap} \tag{1}$$

In Eq. (1), the term $k_p x_p$ denotes the spring force f_p. It can be obtained given the value of spring stiffness k_p and deformation x_p. Symbol D_{ap} denotes the output displacement of the FE SEA and is obtained using

$$x_p = D_p - D_{ap} \tag{2}$$

where D_p is the screw displacement. The gravitational force of the wrist is not considered in Eq. (1) because it can be pre-calculated and compensated for using the motor torques. To develop the AAN controller, we consider a force controller as shown in Fig. 3(b). Given $f_{pr}(s)$ as the reference of f_p, the force control loop includes a proportional gain K_{pp}. The transfer functions H_{11p}, H_{12p}, H_{21p}, and H_{22p} can be derived based on Eqs. (1-2). The force controller is stable based on the Routh–Hurwitz stability criterion. A quick root-locus analysis can show that the relative stability increases when the value of K_{pp} decreases. Although the transient response may not be the best, the proportional controller is used throughout this paper because of the ease of controller development.

Table 1 lists the dynamic and controller parameters of the FE SEA. The values of the reflected motor mass, the damping coefficient, and the efficiency coefficient were identified experimentally. The mass and inertia parameters of the human hand were adapted from [24] while the mass and inertia parameters of the wrist robot were obtained from the CAD model. These parameters are then used to compute the reflected output mass M_{ap} at $\theta_p = 0°$.

TABLE 1. Dynamic and controller parameters of the FE SEA.

Parameter	Value
Reflected motor mass, M_p	19.61 kg
Viscous damping coefficient, ξ	1.515 Ns/mm
Efficiency coefficient, η	0.9248
Reflected output mass, M_{ap}	21.35 kg
Spring stiffness, k_p	23.54 N/mm
Proportional gain, K_{pp}	50

By replacing the subscript p in Eqs. (1-2) and Fig. 3(a) with y, the dynamic equations for the RU rotation can be obtained. Because the equations are similar, the force controller of the FE SEA in Fig. 3(b) can be readily adapted for the RU SEA. The dynamic and controller parameters of the RU SEA are the same as the FE SEA in Table 1 except that $M_{ay} = 16.20$ kg.

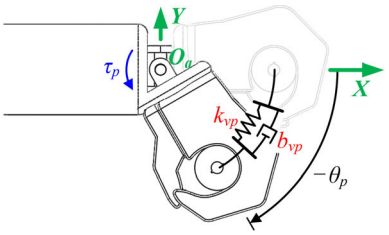

FIGURE 4. Schematic of virtual spring and virtual damper in the FE direction.

B. IMPEDANCE CONTROL

The force controller in Fig. 3(b) can be used to control the interface virtual impedance between the wrist robot and the human hand. Fig. 4 shows a schematic of the human hand and the virtual spring and virtual damper in the FE direction. The rotational stiffness of the virtual spring measured at the wrist center O_a is denoted as k_{vp}, whereas the rotational damping coefficient of the virtual damper is denoted as b_{vp}. Starting from $\theta_p = 0°$, the robot produces an output torque τ_p that is equal to the torque resulting from the elongation of the virtual spring and damper. The rotational stiffness and damping coefficient in the RU direction can be similarly defined as k_{vy} and b_{vy}, respectively. The virtual springs and dampers constitute the virtual impedance that can be controlled by using the FE and RU torques as follows.

$$\begin{bmatrix} \tau_p \\ \tau_y \end{bmatrix} = \begin{bmatrix} -k_{vp}\theta_p - b_{vp}\dot{\theta}_p \\ -k_{vy}\theta_y - b_{vy}\dot{\theta}_y \end{bmatrix} \tag{3}$$

The minus signs in Eq. (3) indicate that the positive direction of the torque τ_p or τ_y is in the opposite direction as the elongation of the virtual spring and velocity of the FE or RU rotations. The actual spring forces of the SEAs can then be

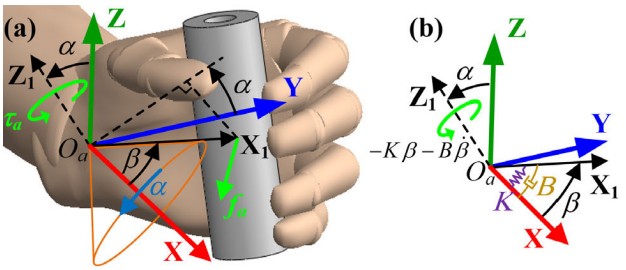

FIGURE 5. (a) Orientation of the wrist and handlebar. (b) Omni-directional stiffness K and omni-directional damping B.

obtained for a given set of τ_p and τ_y.

$$\begin{bmatrix} f_p \\ f_y \end{bmatrix} = \begin{bmatrix} J_p & 0 \\ 0 & J_y \end{bmatrix} \begin{bmatrix} M_{11} & M_{12} \\ 0 & -1 \end{bmatrix}^T \begin{bmatrix} \tau_p \\ \tau_y \end{bmatrix} \tag{4}$$

where J_p, J_y, M_{11}, and M_{12} are determined by the link dimensions of the robot that can be found in [3]. For a given set of k_{vp}, k_{vy}, b_{vp}, and b_{vy}, the required spring forces f_p and f_y can be computed using Eqs. (3-4). The required spring forces f_p is used as the reference spring force f_{pr} of the force controller in Fig. 3(b) (Similarly for f_y and f_{yr}).

IV. ASSIST-AS-NEEDED (AAN) CONTROLLER

A. DESIGN OF THE ASSIST-AS-NEEDED CONTROLLER

To provide the spatial-motion assistance of the wrist, we first need to design a band-type AAN controller for the wrist robot. Considering the case where the predefined equilibrium position is the only zero-impedance position, the wrist robot provides a force in a direction opposite to the intended human limb motion. In the static case, the opposite force is proportional to the distance between the human limb current position and the equilibrium position. The impedance controller presented in Sec. III-B can be treated as a planar-motion AAN controller where only one angle is considered (θ_p or θ_y). Since the human wrist motion includes θ_p and θ_y, a spatial-motion AAN controller is required. If the human hand grips the handlebar firmly, the position of the human wrist can be conveniently represented by a vector $\boldsymbol{X}_1$ from O_a to the center of the handlebar, as shown in Fig. 5(a). The orientation of $\boldsymbol{X}_1$ with respect to the $\boldsymbol{XYZ}$ frame is described by angles α and β, where α is the rotation about $\boldsymbol{X}$ and β is the angle between $\boldsymbol{X}$ and $\boldsymbol{X}_1$. The two angles can be related to θ_p and θ_y by the following.

$$\begin{aligned} \theta_p &= S^{-1}(C_\alpha S_\beta); \quad \theta_y = T^{-1}(-S_\alpha S_\beta / C_\beta) \\ \beta &= C^{-1}(C_y C_p); \quad \alpha = T^{-1}(-S_y C_p / S_p) \end{aligned} \tag{5}$$

where S, C, and T denote the sine, cosine, and tangent functions, respectively. The subscripts of S and C denote angle α, β, θ_p, or θ_y. When β is constant, vector $\boldsymbol{X}_1$ moves on the surface of a cone as shown in Fig. 5(a). As an illustration, Fig. 6 shows the polar plot of α and β where α = 0-360° represents the radial coordinate and β = 0-45° represents the angular coordinate. The origin is at $\alpha = \beta = 0°$. The corresponding configurations of a left wrist at different positions

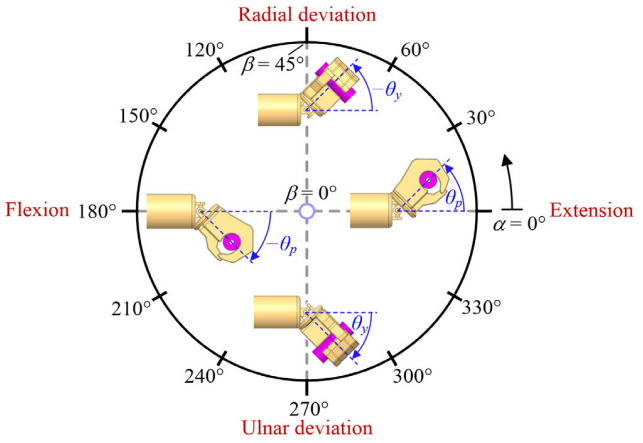

FIGURE 6. Wrist configurations at different values of α and β.

in the polar plot are also shown. The extension, radial deviation, flexion, and ulnar deviation correspond to $\alpha = 0°$, 90°, 180°, and 270°, respectively. At those angles, β is equal to $\pm\theta_p$ or $\pm\theta_y$.

Considering the equilibrium position at $\alpha = \beta = 0°$ (also $\theta_p = \theta_y = 0°$), the wrist robot should provide an assistance torque $\boldsymbol{\tau_a}$ for nonzero α and β that assists the wrist to move back to the equilibrium position. As shown in Fig. 5(a), this torque should be along the $\boldsymbol{Z}_1$ axis with no component on the $\boldsymbol{Y}_1$ axis. Considering an omni-directional stiffness K as illustrated using a torsional spring and an omni-directional damping B as illustrated using a torsional damper in Fig. 5(b), the assistance torque $\boldsymbol{\tau_a}$ in Fig. 5(a) should be equal to $-K\beta - B\dot{\beta}$ in order to create a proportional and opposite assistance force $\boldsymbol{f_a}$ at the handlebar. The assistance torque from the wrist robot can be expressed as $\boldsymbol{\tau_a} = [\tau_p S_y \ \tau_y \ \tau_p C_y]^T$. With this expression, we arrive at the following requirement for τ_p and τ_y.

$$\begin{aligned} \begin{bmatrix} \tau_{Z1} \\ \tau_{Y1} \end{bmatrix} &= \begin{bmatrix} C_y C_\alpha & -S_\alpha \\ C_y S_\alpha C_\beta - S_y S_\beta & C_\alpha C_\beta \end{bmatrix} \begin{bmatrix} \tau_p \\ \tau_y \end{bmatrix} \\ &= \begin{bmatrix} -K\beta - B\dot{\beta} \\ 0 \end{bmatrix} \end{aligned} \tag{6}$$

where τ_{Z1} is the projection of $\boldsymbol{\tau_a}$ on the $\boldsymbol{Z}_1$ axis and τ_{Y1} is the projection of $\boldsymbol{\tau_a}$ on the $\boldsymbol{Y}_1$ axis. Given an omni-directional stiffness K and omni-directional damping B at a specific orientation α and β, the values of τ_p and τ_y can then be computed. Combining Eqs. (4, 6), the required spring forces f_p and f_y from the FE and RU SEAs can be expressed as

$$\begin{bmatrix} f_p \\ f_y \end{bmatrix} = \begin{bmatrix} \dfrac{J_p M_{11} C_\alpha C_\beta}{S_y S_\alpha S_\beta - C_y C_\beta} \\ \dfrac{J_y (M_{12} C_\alpha C_\beta - S_y S_\beta + C_y S_\alpha C_\beta)}{S_y S_\alpha S_\beta - C_y C_\beta} \end{bmatrix} (-K\beta - B\dot{\beta}) \tag{7}$$

The computed f_p and f_y in Eq. (7) may be positive or negative. Same as those in Sec. III-B, the computed spring forces are the reference for the SEA force controller. Later, the values

of τ_{Z1} and τ_{Y1} can be obtained using Eq. (6). The magnitude and direction of the required assistance force $\boldsymbol{f_a}$ to produce the assistance torque $\boldsymbol{\tau_a}$ are computed using

$$|\boldsymbol{f_a}| = \sqrt{f_{Z1}^2 + f_{Y1}^2}; \quad \angle \boldsymbol{f_a} = \alpha - T^{-1}(f_{Y1}/f_{Z1}) + \pi \quad (8)$$

where f_{Z1} and f_{Y1} are the forces to produce the torques τ_{Z1} and τ_{Y1}, respectively. They are related to the associated torques τ_{Z1} and τ_{Y1} by a length L_a, which is the magnitude of $\boldsymbol{X}_1$ and also the distance from the wrist center to the grip center. According to [24], the average value of L_a is nearly 66.8 mm.

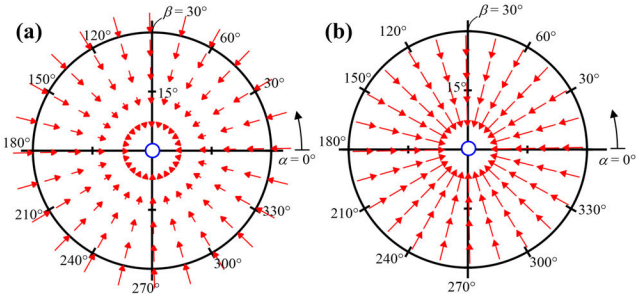

FIGURE 7. (a) Assistance force field of $K = 1$ Nm/rad and $B = 0$. (b) Assistance force field of $C = 0.2$ Nm.

As an illustration, we consider a case where the omni-directional stiffness $K = 1$ Nm/rad and omni-directional damping $B = 0$. Fig. 7(a) shows the polar plot of the ideal $\boldsymbol{f_a}$ where β = 0-30°. At each position (tip of the arrow), the direction and magnitude of each arrow are computed using Eq. (8). The longer the distance from the current position to the origin, the larger the assistance force $\boldsymbol{f_a}$ is. Hence the arrows become longer when they are further away from the origin. Because of the omni-directional stiffness K, any movement of the human's wrist from the origin would result in a force from the wrist robot that attempts to move the wrist back to the origin. The largest force is 7.84 N when $\beta = 30°$.

For the special case of $\alpha = 180°$, the parameters K and B in Fig. 5(b) would be respectively equal to k_{vp} and b_{vp} in Fig. 4.

B. CONSTANT ASSISTANCE TORQUE

When a position-independent constant assistance torque is required instead of a position-dependent virtual impedance, Eq. (6) can be rewritten as follows to meet the requirement.

$$\begin{bmatrix} \tau_{Z1} \\ \tau_{Y1} \end{bmatrix} = \begin{bmatrix} C_y C_\alpha & -S_\alpha \\ C_y S_\alpha C_\beta - S_y S_\beta & C_\alpha C_\beta \end{bmatrix} \begin{bmatrix} \tau_p \\ \tau_y \end{bmatrix} = \begin{bmatrix} -C \\ 0 \end{bmatrix} \quad (9)$$

where C is the omni-directional constant torque from the robot to the human hand. As an illustration, Fig. 7(b) shows the polar plot of the assistance force field when $C = 0.2$ Nm. The magnitude of each arrow is the same ($|\boldsymbol{f_a}| = 3$ N) regardless of the values of α and β.

C. AAN CONTROLLER WITH AN ARBITRARY EQUILIBRIUM POSITION

Based on the band-type AAN controller developed in Sec. IV-A, this section further develops a window-type AAN controller to bridge the gap between active and passive rehabilitation training. When the equilibrium position can be made to move along a time-dependent training trajectory, the force field of the AAN controller acts as the assistance force that moves the wrist along the training trajectory if the wrist cannot follow the trajectory itself. Thus the window-type AAN controller can be treated as a generalization of the band-type AAN controller. In Sec. IV-A, the equilibrium position is at $\alpha = \beta = 0°$. To be used for the AAN controller, we use α_f and β_f to describe an arbitrary equilibrium position that can be specified as a function of time. The output torques required to move the wrist back to $\alpha = \alpha_f$ and $\beta = \beta_f$ can be obtained using the following.

$$\begin{bmatrix} \frac{S_y Z_x + C_y Z_z}{N_d} & \frac{Z_y}{N_d} \\ \frac{S_y Y_x + C_y Y_z}{N_d} & \frac{Y_y}{N_d} \end{bmatrix} \begin{bmatrix} \tau_p \\ \tau_y \end{bmatrix} = \begin{bmatrix} -K\beta_r - B\dot{\beta}_r \\ 0 \end{bmatrix} \quad (10a)$$

where

$$\beta_r = C^{-1}(C_\beta C_{\beta_f} + S_\beta S_{\beta_f} C_{\alpha-\alpha_f}) \quad (10b)$$

Symbol β_r denotes the angle between two vectors. The first vector is at $\alpha = \alpha_f$ and $\beta = \beta_f$, whereas the second vector is at arbitrary α and β. The values of N_d, Y_x, Y_y, Y_z, Z_x, Z_y, and Z_z depend on the angles α, β, α_f, and β_f given as follows.

$$\begin{aligned}
N_d &= [(C_{\alpha_f} S_{\beta_f} S_\alpha S_\beta - S_{\alpha_f} S_{\beta_f} C_\alpha S_\beta)^2 \\
&\quad + (S_{\alpha_f} S_{\beta_f} C_\beta - S_\alpha S_\beta C_{\beta_f})^2 \\
&\quad + (C_{\beta_f} C_\alpha S_\beta - C_\beta C_{\alpha_f} S_{\beta_f})^2]^{1/2} \\
Y_x &= S_\beta (C_{\alpha-\alpha_f} C_\beta S_{\beta_f} - C_{\beta_f} S_\beta) \\
Y_y &= S_{\beta_f} (S_\alpha S_\beta^2 S_{\alpha_f-\alpha} - C_{\alpha_f} C_\beta^2) + C_{\beta_f} C_\alpha S_\beta C_\beta \\
Y_z &= C_{\beta_f} S_\alpha S_\beta C_\beta - S_{\alpha_f} S_{\beta_f} C_\beta^2 + S_{\beta_f} S_{\alpha-\alpha_f} C_\alpha S_\beta^2 \\
Z_x &= C_{\alpha_f} S_{\beta_f} S_\alpha S_\beta - S_{\alpha_f} S_{\beta_f} C_\alpha S_\beta \\
Z_y &= S_{\alpha_f} S_{\beta_f} C_\beta - S_\alpha S_\beta C_{\beta_f} \\
Z_z &= C_{\beta_f} C_\alpha S_\beta - C_\beta C_{\alpha_f} S_{\beta_f}
\end{aligned} \quad (10c)$$

Similar to the derivation in Sec. IV-A, the required spring forces f_p and f_y can be expressed as

$$\begin{bmatrix} f_p \\ f_y \end{bmatrix} = \begin{bmatrix} J_p M_{11} Y_y \\ J_y (M_{12} Y_y + S_y Y_x + C_y Y_z) \end{bmatrix} \frac{N_d}{H} (-K\beta_r - B\dot{\beta}_r)$$
$$\text{where } H = (S_y Y_x + C_y Y_z) Z_y - (S_y Z_x + C_y Z_z) Y_y \quad (11)$$

The required spring forces f_p and f_y need to vary according to the given α_f, β_f, K, and B. The required spring forces are then used as the reference for the force controller in Fig. 3(b). If directional stiffness and damping are required, K and B in Eq. (11) can be specified as functions of α.

As an illustration, we consider a case with $\alpha_f = 225°$, $\beta_f = 17°$, $K = 1$ Nm/rad, and $B = 0$. Fig. 8 shows the polar plot of the assistance force. The red arrows indicate the ideal assistance force. The arrows all point toward the new equilibrium position α_f and β_f.

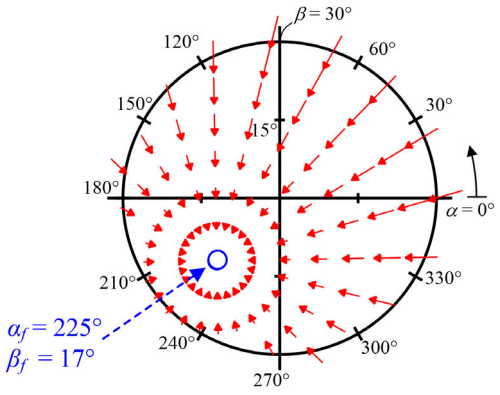

FIGURE 8. Assistance force field when $\alpha_f = 225°$ and $\beta_f = 17°$.

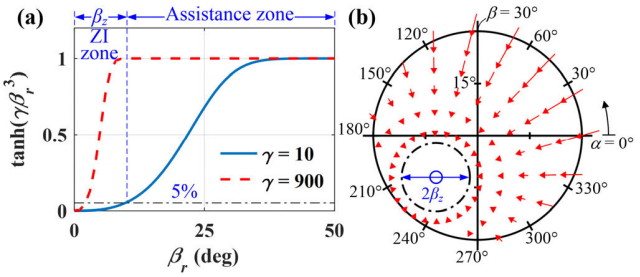

FIGURE 9. (a) Smoothing function using the hyperbolic tangent. (b) Assistance force field when the smoothing function is applied.

D. ZERO IMPEDANCE (ZI) ZONE AND SMOOTHING FUNCTION

For the window-type AAN controller, a zero impedance (ZI) zone is required to define the condition when the robot assistance is not needed. To transfer between the ZI zone and assistance zone, a smoothing function is required to modify the spring forces f_p and f_y. Without loss of generality, we consider here a smoothing function using the hyperbolic tangent.

$$[f_{pr} \;\; f_{yr}]^T = \tanh(\gamma\beta_r^3)[f_p \;\; f_y]^T \tag{12}$$

where f_{pr} and f_{yr} are the modified spring forces that are to be used as the references of the FE and RU force controllers. Parameter γ is used to characterize the size of the ZI zone. Fig. 9(a) shows an illustration of $\gamma = 10$ and $\gamma = 900$. We define the ZI zone as the range of β_r when the absolute value of $\tanh(\gamma\beta_r^3)$ is less than 0.05. This ZI zone has a radius of β_z that can be calculated using

$$\beta_z = [\tanh^{-1}(0.05)/\gamma]^{1/3} \tag{13}$$

Hence the radii of the ZI zones of $\gamma = 10$ and $\gamma = 900$ are 9.8° and 2.2°, respectively. For the same β_r outside the ZI zone, the value of the spring force is larger if γ is larger. Hence the assistance force from the robot is larger. When γ approaches infinity, the radius of the ZI zone approaches zero.

As an illustration, Fig. 9(b) shows the assistance force field when a smoothing function of $\gamma = 10$ is applied to the force filed in Fig. 8. Inside the ZI zone with a diameter of $2\beta_z$, the robot offers almost no assistance. The assistance force outside the ZI zone depends on the values of K and B as well as the distance from the equilibrium position.

E. AAN CONTROLLER DIAGRAM AND STABILITY ANALYSIS

In summary, K, B, γ, α_f, and β_f are the essential parameters of the AAN controller. The strength of the assistance force depends on K and B, whereas the range of the ZI zone depends on γ. The center position of the ZI zone further depends on α_f and β_f. These parameters can be adjusted online to meet the progress and need of each participant.

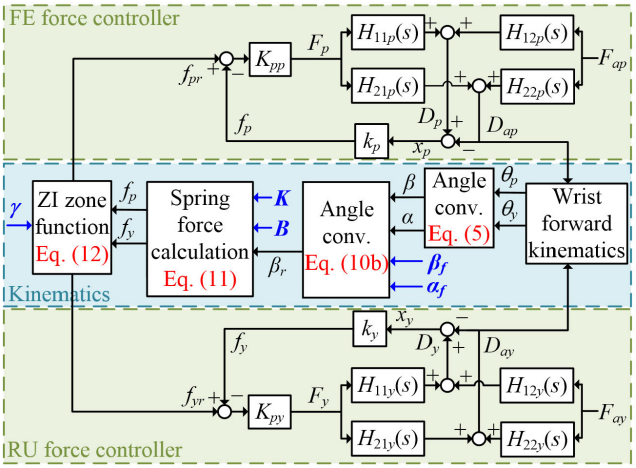

FIGURE 10. AAN controller diagram.

Fig. 10 shows the AAN controller diagram. Given the parameters K, B, γ, α_f, and β_f, the reference spring forces f_{pr} and f_{yr} can be computed using the kinematic equations in Eqs. (10b), (11), and (12). As shown in the middle block in Fig. 10, these two reference forces are used as the input for the FE and RU force controllers in the top and bottom blocks, respectively. They may act in the same or opposite directions as F_{ap} and F_{ay} from the human wrist. The force controllers were implemented using the field-programmable-gate-array (FPGA) module in NI cRIO 9039 with a sampling frequency of 1 kHz. The middle block in Fig. 10 was implemented using the real-time (RT) module in NI cRIO 9039.

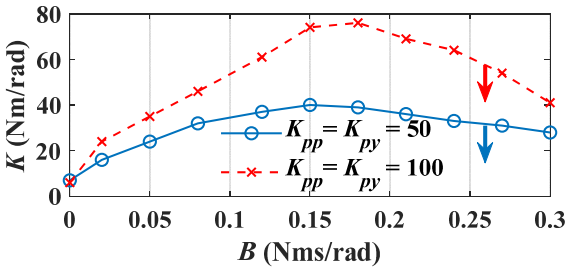

FIGURE 11. Stability analysis of the AAN controller.

The stability of the AAN controller depends on K and B. Fig. 11 shows the stability diagram of the controller with respect to different values of K and B. Two sets of force

controller gains (K_{pp} and K_{py}) are studied. The area under each curve represents the stable region where the values of K and B can be selected. Values of K and B outside the stable region would cause instability. The curve of $K_{pp} = K_{py} = 100$ has a larger stable region when compared with the curve of $K_{pp} = K_{py} = 50$. When $B = 0$, the maximum allowable value of K is 6 Nm/rad regardless of the controller gains and reflected masses (M_{ap} and M_{ay}). Larger values of k_p and k_y can be applied to increase the maximum allowable value of K at $B = 0$. For both simplicity and stability concerns, the following section on experimental verifications uses $K =$ 0-3 Nm/rad, $B = 0$, and $K_{pp} = K_{py} = 50$. If larger values of K are required, the values of B, K_{pp}, and K_{py} should be increased to further ensure stability.

V. EXPERIMENTAL VERIFICATIONS

This section provides four different experiments to illustrate that the proposed AAN controller could be used for passive, assist-as-needed, active, and resistive rehabilitation trainings. These training exercises can be sequentially used for participants of neuromuscular injury from the initial stage where there is no muscle function (passive) to the final stage where the muscle function returns (active or resistive). Thus the proposed AAN controller can be used for the wrist robot to cover the entire Bruunstrom stages. The only adaptation required is the different set of parameters K, B, γ, α_f, and β_f for each stage of rehabilitation exercise.

TABLE 2. AAN controller parameters for each rehabilitation stage.

Stage	K (Nm/rad)	γ	α_f and β_f	Subsection
Passive	3	∞	Trajectory dependent	V-A
Assist-as-needed	0-3	10-900	Trajectory dependent	V-B
Active	0	0	(0, 0)	V-C
Resistive	0-3	∞	(0, 0)	V-D

Because the wrist rehabilitation motion is relatively slow, manipulating the value of K to adjust the assistance or resistance force would be more significant than to manipulate the value of B. Hence we mainly focus on the effect of K in the following experiments. Table 2 lists the range of the parameters for each stage of rehabilitation training. When $K = 3$ Nm/rad, the human wrist needs to produce a torque of 0.35 Nm in order to rotate 6.7°. This torque value is considered to be very high for activities of daily living [25]. Hence setting K to 3 Nm/rad would sufficiently create a stiff environment for passive rehabilitation. In addition, it was reported in [26] that the human maximum passive wrist stiffness is 3 Nm/rad. Thus a K value no more than 3 Nm/rad could avoid a participant's potential injury.

Depending on the required robot force intensity, the value of K in the assist-as-needed or resistive rehabilitation stage can vary between 0 and 3 Nm/rad. The value of γ can also vary in the assist-as-needed stage but needs to be ∞ ($\beta_z = 0$) in the passive and resistive stages while 0 ($\beta_z = \infty$) in the active stage. When changing between different rehabilitation stages in the middle of the exercise is required, smooth transitions of the values of K, B, γ, α_f, and β_f should be made.

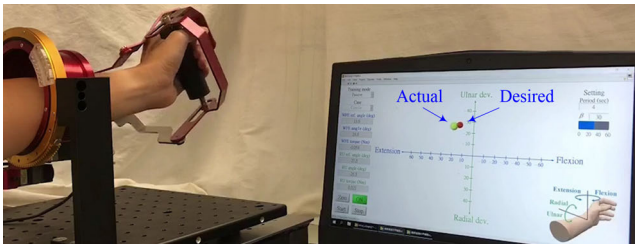

FIGURE 12. Experimental setup.

Fig. 12 shows the experimental setup. The experiments in this section mainly involve a healthy female participant (P_1) that is 163 cm tall and weighs 54 kg. A computer screen was provided for the participant to visually trace the trajectory. The red and green dots on the screen denote the desired (α_f and β_f) and actual (α and β) trace points, respectively.

A. EXPERIMENT OF PASSIVE REHABILITATION

Passive rehabilitation is used when the human wrist activity is ignored and the robot is fully in charge of the motion. To accurately control the wrist motion, the omni-directional stiffness K needs to be large enough while the size of the ZI zone needs to be zero ($\beta_z = 0$) in order to constrain the motion of the human wrist. In the experiment, the participant was asked to hold the handlebar and relax her wrist.

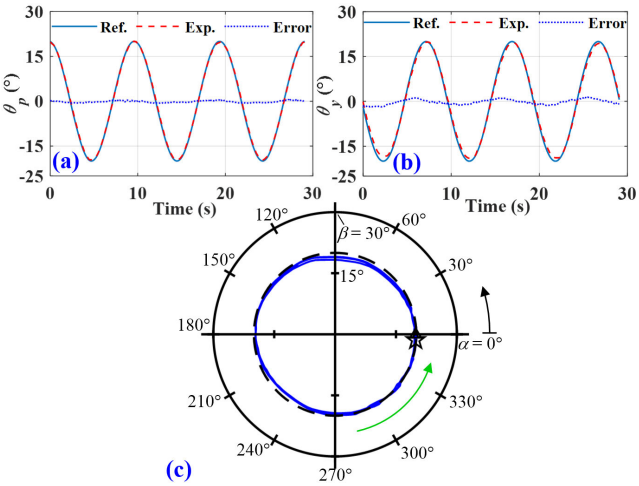

FIGURE 13. Passive rehabilitation: (a) Experimental FE rotation curve. (b) Experimental RU rotation curve (c) Rotation trajectory ($K = 3$ Nm/rad, $\gamma = \infty$, $\alpha_f = time \times 36°$, and $\beta_f = 20°$).

Fig. 13 shows the experimental results of passive rehabilitation where $\alpha_f = time \times 36°$ and $\beta_f = 20°$ were used for the controller in Fig. 10. The rotation trajectory in Fig. 13(c)

shows that the human wrist can be controlled to follow the desired trajectory. In Fig. 13(a) and 13(b), the reference angles of θ_p and θ_y are computed using Eq. (5). The differences between the reference and experimental angle curves are quite small. The root mean square (RMS) errors are 0.362° and 0.847°, respectively. The errors are primarily due to the passive stiffness originated from the human wrist. Using a larger value of K would force the human wrist to follow more strictly along the desired trajectory. However, a too large K may cause wrist injury.

If spasticity develops during the passive rehabilitation, the actual wrist trajectory will deviate from the desired trajectory. The speed of moving on the desired trajectory and stiffness K can be adjusted to evaluate the treatment of spasticity.

B. EXPERIMENT OF ASSIST-AS-NEEDED REHABILITATION

The participant's left hand holds the handlebar. Using $\alpha_f = time \times 36°$ and $\beta_f = 30°$ to describe the time-dependent circular trajectory, seven cycles were tested. Each cycle lasted for ten seconds. For the first three cycles, the participant was instructed to relax and remain passive. For the last three cycles, the participant was instructed to actively trace the desired circular trajectory. The fourth cycle was used for the transition from passive to active. Fig. 14(a) and 14(b) show the experimental wrist trajectories of $\gamma = 10$ and $\gamma = 900$, respectively. Both cases have $K = 1$ Nm/rad. The trajectories of the first three and last three cycles are shown in blue and red lines, respectively. The desired trajectory is shown in black dashed line. When the participant's wrist is passive, the handlebar can still trace the circular path due to robot assistance. Because the ZI zone of $\gamma = 900$ is smaller than that of $\gamma = 10$, the controller of $\gamma = 900$ is stricter and the robot provides more assistance force at the same handlebar position. Hence the blue line in Fig. 14(b) is closer to the desired trajectory, whereas the blue line in Fig. 14(a) deviates from the desired trajectory. When the participant's wrist engages actively, the robot offers no assistance and the red lines in Fig. 14(a) and 14(b) are both near the desired trajectory.

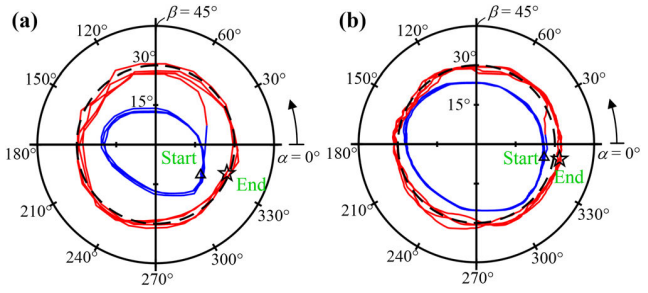

FIGURE 14. Experimental wrist trajectory of assist-as-needed rehabilitation: (a) $\gamma = 10$, $K = 1$ Nm/rad (b) $\gamma = 900$, $K = 1$ Nm/rad.

Fig. 15 shows the output FE and RU torques associated with Fig. 14(b) where $\gamma = 900$. The output torques are

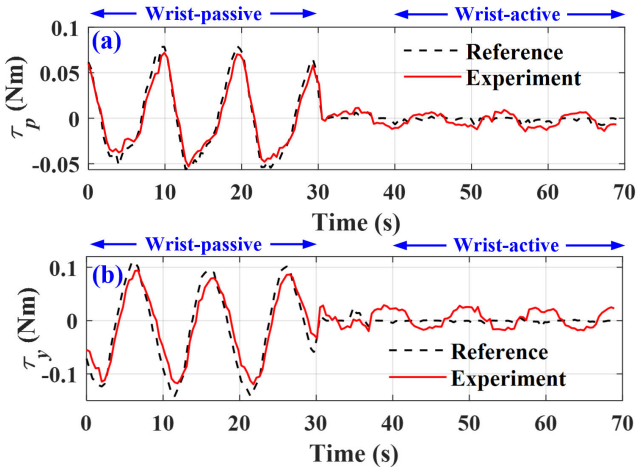

FIGURE 15. (a) Experimental FE torque curve of $\gamma = 900$. (b) Experimental RU torque curve of $\gamma = 900$.

computed using Eq. (4). Both the FE and RU torques are larger in the wrist-passive period when compared with those in the wrist-active period. In the wrist-active period, the robot provides almost no torque because the human wrist is able to follow the desired trajectory without assistance. For both subfigures, the experimental torque curves match well with the reference ones. This demonstrates the accuracy of the AAN controller that uses the proposed FE and RU SEAs in Sec. II. The small fluctuation of the FE experimental torque curves in the wrist-active period is less than 0.01 Nm, which is very small and close to the force controller's response limit. If the participant suddenly stops following the trajectory during the wrist-active period, the robot will go back to the wrist-passive mode.

The output FE and RU torques associated with Fig. 14(a) can also be shown. Because γ is smaller, the ZI zone is larger. The assistance torque in the wrist-passive period would be smaller than that of $\gamma = 900$. Depending on the progress of rehabilitation, the parameter γ can be used to adjust the size of the assistance region provided by the wrist robot.

TABLE 3. Root mean square values of the FE and RU torques (Nm).

Participant and period	FE ($\gamma = 10$)	RU ($\gamma = 10$)	FE ($\gamma = 900$)	RU ($\gamma = 900$)
P_1, wrist-passive	0.031	0.047	0.038	0.070
P_1, wrist-active	0.008	0.017	0.008	0.017
P_2, wrist-passive	0.086	0.123	0.107	0.171
P_2, wrist-active	0.025	0.032	0.028	0.040

An additional healthy male participant (P_2) was involved in the same assist-as-needed experiment. The male participant is 174 cm tall and weighs 74 kg. Table 3 lists the root mean square values of the output FE and RU torques with respect to different participants (P_1 and P_2), different

periods (wrist-active and wrist-passive), and different values of γ (10 and 900). The AAN controller provides different torques for each participant in the wrist-passive period. The contribution of the FE and RU torques is only necessary to assist each participant to follow the desired trajectory.

C. EXPERIMENT OF ACTIVE REHABILITATION

By setting $K = 0$ Nm/rad, $\gamma = 0$, $\alpha_f = 0°$, and $\beta_f = 0°$ for the controller in Fig. 10, the wrist robot becomes completely back-drivable and transparent. This setting is denoted as the active rehabilitation where only the human wrist is active and the robot is not. The active rehabilitation can be used to evaluate the active range of motion of a recovering human wrist. The same participant (P_1) was asked to rotate her wrist repeatedly in a comfortable range of motion. Fig. 16 shows the experimental results of active rehabilitation. In Fig. 16(c), the polar plot shows that the wrist rotates diagonally at an amplitude of $\beta = 30°$. The output torques τ_p and τ_y are shown in Fig. 16(a) and 16(b), respectively. The associated output angles vary sinusoidally at 0.5 Hz. Due to zero K, both τ_p and τ_y are controlled to be very small regardless of the variation of θ_p and θ_y. The root mean square values of τ_p and τ_y are 0.006 Nm and 0.02 Nm, respectively. These values also match with those obtained using simulation (not shown in Fig. 16(a) and 16(b) for the sake of clarity). The almost zero resistance from the robot allows accurate assessment of active wrist range of motion.

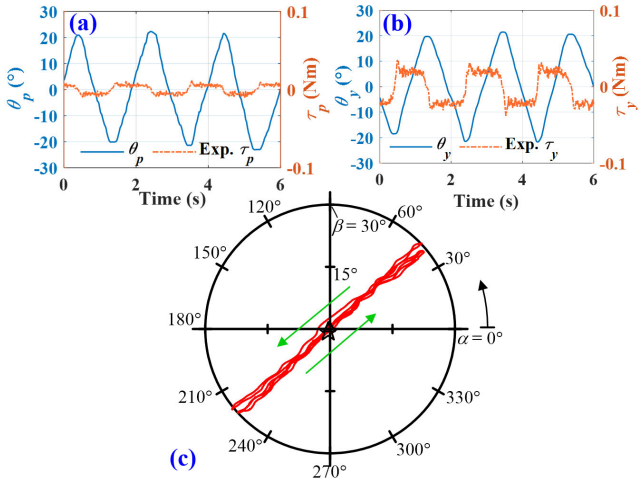

FIGURE 16. Active rehabilitation: (a) Experimental FE rotation and torque curves. (b) Experimental RU rotation and torque curves. (c) Rotation trajectory ($K = 0$ Nm/rad, $\gamma = 0$, $\alpha_f = 0°$, and $\beta_f = 0°$, 0.5 Hz).

D. EXPERIMENT OF RESISTIVE REHABILITATION

When a participant gradually recovers his/her wrist function, a resistive training is required to further strengthen his/her muscle force and speed. To demonstrate the AAN controller for the resistive rehabilitation, an experiment has been conducted. In the experiment, the participant's hand held the handlebar and rotated manually to overcome the assistance force provided by the wrist robot ($K = 1$ Nm/rad).

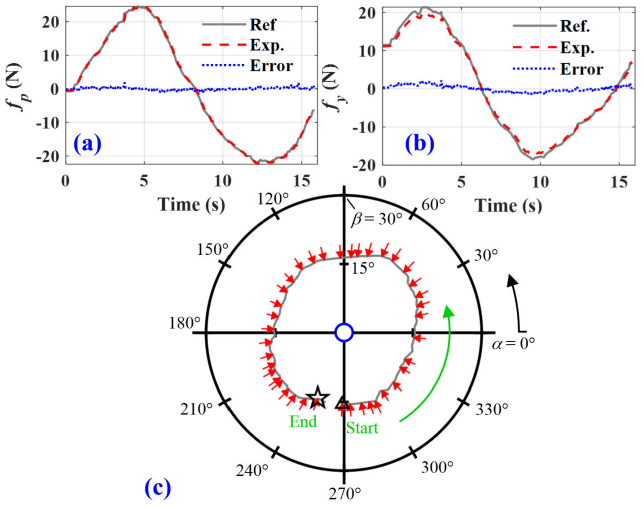

FIGURE 17. Resistive rehabilitation: (a) Experimental FE spring force curve. (b) Experimental RU spring force curve. (c) Experimental assistance force field and trajectory of the handlebar ($K = 1$ Nm/rad, $\gamma = \infty$, $\alpha_f = 0°$, and $\beta_f = 0°$).

The displacements D_{ap} and D_{ay} and SEA spring deformations x_p and x_y were recorded. These values were used to obtain the spring forces f_p and f_y. Fig. 17(a) and 17(b) show the FE and RU spring forces, respectively. The reference spring force curves are computed using Eqs. (11-12). Because of the very small root mean square error of the spring force (less than 0.2 N), the experimental force curves match well with the reference force curves. This demonstrates the accuracy of the AAN controller. Fig. 17(c) further shows the trajectory of the handlebar. Starting from the triangular mark, the handlebar moves counterclockwise to reach the star mark. The force vectors are also plotted at every 0.4 second. The force pattern is very similar to that in Fig. 17(a). By adjusting the values of K and B, this spatial-motion AAN controller can be used to train a participant's wrist muscle at different intensities.

VI. CONCLUSIONS

This paper has presented a spatial-motion AAN controller to provide the robotic wrist motion required for all the rehabilitation stages. The AAN controller includes an omni-directional stiffness K that determines the strength of the assistance force and a ZI zone parameter γ that determines the amount of area that needs assistance. These two parameters can be adaptively adjusted to meet the progress and need of each participant.

By adjusting the controller parameters K and γ, the AAN controller has been experimentally demonstrated to provide various human wrist rehabilitations that includes passive, assist-as-needed, active, and resistive motion. We expect that the proposed controller framework can be extended to develop similar AAN controllers for the total robotic rehabilitation of other multi-DoF joints such as the human shoulder or ankle.

REFERENCES

[1] H.-C. Hsieh, D.-F. Chen, L. Chien, and C.-C. Lan, "Design of a parallel actuated exoskeleton for adaptive and safe robotic shoulder rehabilitation," *IEEE/ASME Trans. Mechatronics*, vol. 22, no. 5, pp. 2034–2045, Oct. 2017.
[2] A. Mancisidor, A. Zubizarreta, I. Cabanes, P. Bengoa, A. Brull, and J. H. Jung, "Inclusive and seamless control framework for safe robot-mediated therapy for upper limbs rehabilitation," *Mechatronics*, vol. 58, pp. 70–79, Apr. 2019.
[3] Y.-Y. Su, Y.-L. Yu, C.-H. Lin, and C.-C. Lan, "A compact wrist rehabilitation robot with accurate force/stiffness control and misalignment adaptation," *Int. J. Intell. Robot. Appl.*, vol. 3, no. 1, pp. 45–58, Mar. 2019.
[4] H. I. Krebs, B. T. Volpe, D. Williams, J. Celestino, S. K. Charles, D. Lynch, and N. Hogan, "Robot-aided neurorehabilitation: A robot for wrist rehabilitation," *IEEE Trans. Neural Syst. Rehabil. Eng.*, vol. 15, no. 3, pp. 327–335, Sep. 2007.
[5] A. Gupta, M. K. O'Malley, V. Patoglu, and C. Burgar, "Design, control and performance of RiceWrist: A force feedback wrist exoskeleton for rehabilitation and training," *Int. J. Robot. Res.*, vol. 27, no. 2, pp. 233–251, 2008.
[6] E. Akdoğan, M. E. Aktan, A. T. Koru, M. S. Arslan, M. Atlihan, and B. Kuran, "Hybrid impedance control of a robot manipulator for wrist and forearm rehabilitation: Performance analysis and clinical results," *Mechatronics*, vol. 49, pp. 77–91, Feb. 2018.
[7] D. Buongiorno, E. Sotgiu, D. Leonardis, S. Marcheschi, M. Solazzi, and A. Frisoli, "WRES: A novel 3 DoF WRist ExoSkeleton with tendon-driven differential transmission for neuro-rehabilitation and teleoperation," *IEEE Robot. Automat. Lett.*, vol. 3, no. 3, pp. 2152–2159, Jul. 2018.
[8] E. T. Wolbrecht, V. Chan, D. J. Reinkensmeyer, and J. E. Bobrow, "Optimizing compliant, model-based robotic assistance to promote neurorehabilitation," *IEEE Trans. Neural Syst. Rehabil. Eng.*, vol. 16, no. 3, pp. 286–297, Jun. 2008.
[9] A. U. Pehlivan, F. Sergi, and M. K. OMalley, "A subject-adaptive controller for wrist robotic rehabilitation," *IEEE/ASME Trans. Mechatronics*, vol. 20, no. 3, pp. 1338–1350, Jun. 2015.
[10] T. Teramae, T. Noda, and J. Morimoto, "EMG-based model predictive control for physical human–robot interaction: Application for assist-as-needed control," *IEEE Robot. Automat. Lett.*, vol. 3, no. 1, pp. 210–217, Jan. 2018.
[11] E. Vergaro, M. Casadio, V. Squeri, P. Giannoni, P. Morasso, and V. Sanguineti, "Self-adaptive robot training of stroke survivors for continuous tracking movements," *J. Neuroeng. Rehabil.*, vol. 7, no. 1, p. 13, Dec. 2010.
[12] Q. Wu, B. Chen, and H. Wu, "Adaptive admittance control of an upper extremity rehabilitation robot with Neural-Network-Based disturbance observer," *IEEE Access*, vol. 7, pp. 123807–123819, 2019.
[13] S. Li, J. Li, G. Tian, and H. Shang, "Stiffness adjustment for a single-link robot arm driven by series elastic actuator in muscle training," *IEEE Access*, vol. 7, pp. 65029–65039, 2019.
[14] T. Wang, Y. Zhu, T. Zheng, D. Sui, S. Zhao, and J. Zhao, "PALExo: A parallel actuated lower limb exoskeleton for high-load carrying," *IEEE Access*, vol. 8, pp. 67250–67262, 2020.
[15] A. Duschau-Wicke, A. Caprez, and R. Riener, "Patient-cooperative control increases active participation of individuals with SCI during robot-aided gait training," *J. Neuroeng. Rehabil.*, vol. 7, no. 1, p. 43, Dec. 2010.
[16] H. J. Asl, T. Narikiyo, and M. Kawanishi, "An assist-as-needed control scheme for robot-assisted rehabilitation," in *Proc. Amer. Control Conf. (ACC)*, 2017, pp. 198–203.
[17] P. G. Vinoj, S. Jacob, V. G. Menon, S. Rajesh, and M. R. Khosravi, "Brain-controlled adaptive lower limb exoskeleton for rehabilitation of post-stroke paralyzed," *IEEE Access*, vol. 7, pp. 132628–132648, 2019.
[18] M. Zhang, A. McDaid, A. J. Veale, Y. Peng, and S. Q. Xie, "Adaptive trajectory tracking control of a parallel ankle rehabilitation robot with joint-space force distribution," *IEEE Access*, vol. 7, pp. 85812–85820, 2019.
[19] K. A. Sawner, J. M. LaVigne, and S. Brunnstrom, *Brunnstrom's Movement Therapy in Hemiplegia: A Neurophysiological Approach*. New York, NY, USA: Lippincott, 1992.
[20] K.-Y. Wu, Y.-Y. Su, Y.-L. Yu, C.-H. Lin, and C.-C. Lan, "A 5-Degrees-of-Freedom lightweight elbow-wrist exoskeleton for forearm fine-motion rehabilitation," *IEEE/ASME Trans. Mechatronics*, vol. 24, no. 6, pp. 2684–2695, Dec. 2019.
[21] S. Pareek, H. Manjunath, E. T. Esfahani, and T. Kesavadas, "MyoTrack: Realtime estimation of subject participation in robotic rehabilitation using sEMG and IMU," *IEEE Access*, vol. 7, pp. 76030–76041, 2019.
[22] L. Bai, M. G. Pepper, Y. Yan, M. Phillips, and M. Sakel, "Low cost inertial sensors for the motion tracking and orientation estimation of human upper limbs in neurological rehabilitation," *IEEE Access*, vol. 8, pp. 54254–54268, 2020.
[23] K.-Y. Lin, C.-C. Chung, and C.-C. Lan, "Improving the dynamic force control of series elastic actuation using motors of high Torque-to-Inertia ratios," *IEEE Access*, vol. 8, pp. 6968–6977, 2020.
[24] R. F. Chandler, C. E. Clauser, J. T. McConville, H. M. Reynolds, and J. W. Young, "Investigation of inertial properties of the human body," Air Force Res. Lab., Wright-Patterson Air Force Base, OH, USA, Tech. Rep. AMRL-TR-74-137, 1975.
[25] J. Rosen, J. C. Perry, N. Manning, S. Burns, and B. Hannaford, "The human arm kinematics and dynamics during daily activities-toward a 7 DOF upper limb powered exoskeleton," in *Proc. 12th Int. Conf. Adv. Robot.*,Jul. 2005, pp. 532–539.
[26] D. Formica, S. K. Charles, L. Zollo, E. Guglielmelli, N. Hogan, and H. I. Krebs, "The passive stiffness of the wrist and forearm," *J. Neurophysiol.*, vol. 108, no. 4, pp. 1158–1166, Aug. 2012.

CHING-HUI LIN received the B.S. degree in mechanical engineering from National Chung Cheng University, Taiwan, in 2017, and the M.S. degree from National Cheng Kung University, Taiwan, in 2020. Her previous research interests were control systems, mechatronics, and robotics.

YIN-YU SU received the B.S. and M.S. degrees in mechanical engineering from National Cheng Kung University, Taiwan, in 2016 and 2019, respectively. His previous research interests were mechanism design, robotics, and exoskeletons.

YU-HSUAN LAI received the B.S. degree in mechanical engineering from National Chung Cheng University, Taiwan, in 2019. She is currently pursuing the M.S. degree in mechanical engineering with National Cheng Kung University, Taiwan. Her current research interests are control systems, mechatronics, and rehabilitation robots.

CHAO-CHIEH LAN (Senior Member, IEEE) received the B.S. degree in mechanical engineering from National Taiwan University, Taiwan, in 2000, and the Ph.D. degree in mechanical engineering from the Georgia Institute of Technology, in 2006. He is currently a Professor with the Department of Mechanical Engineering, National Cheng Kung University, Taiwan. He is currently interested in compliant actuators, robotics, mechanism dynamics, and rehabilitation devices.